

X-rays from the redshift 7.1 quasar ULAS J1120+0641

M.J. Page¹, C. Simpson², D.J. Mortlock^{3,4}, S.J. Warren³, P.C. Hewett⁵,
B.P. Venemans⁶ and R.G. McMahon⁵

¹Mullard Space Science Laboratory, University College London, Holmbury St Mary, Dorking, Surrey, RH5 6NT, UK

²Astrophysics Research Institute, Liverpool John Moores University, Liverpool Science Park, 146 Brownlow Hill, Liverpool L3 5RF, UK

³Astrophysics Group, Imperial College London, Blackett Laboratory, Prince Consort Road, London, SW7 2AZ, UK

⁴Department of Mathematics, Imperial College London, London, SW7 2AZ, UK

⁵Institute of Astronomy, University of Cambridge, Madingley Road, Cambridge CB3 0HA, UK

⁶Max-Planck Institute for Astronomy, Königstuhl 17, 69117 Heidelberg, Germany

Accepted 2014 January 29. Received 2014 January 23; in original form 2013 November 07

ABSTRACT

We present X-ray imaging and spectroscopy of the redshift $z = 7.084$ radio-quiet quasar ULAS J112001.48+064124.3 obtained with *Chandra* and *XMM-Newton*. The quasar is detected as a point source with both observatories. The *Chandra* observation provides a precise position, confirming the association of the X-ray source and the quasar, while a sufficient number of photons is detected in the *XMM-Newton* observation to yield a meaningful X-ray spectrum. In the *XMM-Newton* observation the quasar has a 2–10 keV luminosity of $4.7 \pm 0.9 \times 10^{44}$ erg s⁻¹ and a spectral slope $\alpha = 1.6_{-0.3}^{+0.4}$ (where $f_\nu \propto \nu^{-\alpha}$). The quasar appears to have dimmed in the 15 months between the two observations, with a 2–10 keV luminosity of $1.8_{-0.7}^{+1.0} \times 10^{45}$ erg s⁻¹ during the *Chandra* observation. We derive optical to X-ray spectral slopes α_{OX} of 1.76 ± 0.07 and $1.54_{-0.08}^{+0.09}$ at the times of the *XMM-Newton* and *Chandra* observations respectively, consistent with the range of α_{OX} found in other quasars of comparable ultraviolet luminosity. The very soft X-ray spectrum suggests that the quasar is accreting above the Eddington rate, $L/L_{\text{Edd}} = 5_{-4}^{+15}$, compared to $L/L_{\text{Edd}} = 1.2_{-0.5}^{+0.6}$ derived from the rest-frame ultraviolet. Super-Eddington accretion would help to reduce the discrepancy between the age of the quasar implied by the small size of the ionized near zone in which it sits ($< 10^7$ years), and the characteristic e-folding time (2.5×10^7 years if $L/L_{\text{Edd}} = 2$). Such super-Eddington accretion would also alleviate the challenging constraints on the seed black hole mass provided that the quasar has been rapidly accreting throughout its history. The remnant of an individual population III star is a plausible progenitor if an average $L/L_{\text{Edd}} > 1.46$ has been maintained over the quasar’s lifetime.

Key words: quasars: individual: ULAS J1120+0641

1 INTRODUCTION

The dark ages of the Universe, that followed recombination, ended when the ultraviolet (UV) radiation from the first luminous objects reionized the intergalactic medium. It was during this epoch of reionization, which ended at a redshift $z \sim 6$ (Fan et al., 2006), that the first massive black holes blazed as quasars and the first star-forming galaxies assembled. For quasars in particular, the epoch of reionization offers insights and constraints into the process by which massive black holes are formed. An accreting black hole growing at the Eddington rate with a radiative efficiency of 10 per

cent has a mass e-folding timescale (also known as the Salpeter time; Salpeter, 1964) of 5×10^7 years¹.

For the highest redshift quasar yet found, ULAS J112001.48+064124.3 (hereafter ULAS J1120+0641; Mortlock et al., 2011), only 13 such e-folding times have elapsed, corresponding to a factor of 4.4×10^5 increase in mass, between $z = 30$, the earliest epoch at which stars are thought to have formed (Bromm et al., 2009), and $z = 7.084$, at which the quasar is observed (Venemans et al., 2012). The mass of the black hole in ULAS J1120+0641 has been esti-

¹ The e-folding timescale for Eddington-limited accretion is $\tau = \epsilon c \sigma_{\text{T}} / (4\pi G(1 - \epsilon)m_p)$, where ϵ is the efficiency and σ_{T} is the Thomson cross section.

mated from the Mg II emission line in two studies, yielding $2.0^{+1.5}_{-0.7} \times 10^9 M_{\odot}$ (Mortlock et al., 2011) and $2.4 \pm 0.2 \times 10^9 M_{\odot}$ (De Rosa et al., 2013) but note that in this latter case the uncertainties do not include the systematic uncertainty inherent in the estimation method. Both studies find that the bolometric luminosity is consistent with the Eddington luminosity: Mortlock et al. (2011) find $L/L_{\text{Edd}} = 1.2^{+0.6}_{-0.5}$, while De Rosa et al. (2013) find $L/L_{\text{Edd}} = 0.5$ with a factor of 2 systematic error. The deepest upper limit on the radio emission from ULAS J1120+0641 implies that the 1.4 GHz to 4400 Å rest-frame flux density ratio is $R_{1.4}^* < 4.3$, classifying the source as radio-quiet (Momjian et al., 2014). Assuming a black-hole mass of $2.4 \times 10^9 M_{\odot}$, ULAS J1120+0641 would have required a seed black hole of $5.4 \times 10^3 M_{\odot}$ if it grew under Eddington-limited accretion at an efficiency of 10 per cent for the entire period. Thus ULAS J1120+0641 offers challenging constraints for the progenitor black holes of active galactic nuclei (AGN), the rate at which they can grow, or both.

X-ray emission is an ubiquitous property of AGN, emanating from a corona of the inner accretion disc, within a few hundred Schwarzschild radii of the massive black hole. In this paper we present X-ray observations of ULAS J1120+0641 and consider their implications for its accretion rate and growth history. In Section 2 we detail the observations and the data reduction. The results are presented in Section 3. The X-ray emission properties of the quasar are discussed and conclusions are drawn in Section 4. Throughout we adopt the cosmological parameters from the Planck Collaboration (2013): $H_0 = 67.3 \text{ km s}^{-1}$, $\Omega_{\Lambda} = 0.685$ and $\Omega_{\text{m}} = 0.315$. We define power law spectral indices α such that $f_{\nu} \propto \nu^{-\alpha}$ (the equivalent form in terms of the photon index Γ is defined as $N(E) \propto E^{-\Gamma}$ where $\Gamma = \alpha + 1$). X-ray fluxes and luminosities have been corrected for Galactic absorption equivalent to $N_{\text{H}} = 5.07 \times 10^{20} \text{ cm}^{-2}$ (Kalberla et al., 2005). Unless stated otherwise, all uncertainties are given at 1σ .

2 OBSERVATIONS AND DATA REDUCTION

2.1 *Chandra*

ULAS J1120+0641 was observed on 2011 February 4 for 16 ks with *Chandra*. The target fell on the Advanced CCD Imaging Spectrometer (ACIS) S3 chip, which was operated in full-frame, timed-exposure mode, with faint telemetry format. The data were processed with CIAO version 4.5 (Fruscione et al., 2006) and registered to the Sloan Digital Sky Survey (SDSS) Data Release 9 (Ahn et al., 2012) astrometric frame by correlating the positions of X-ray sources with SDSS sources. An image was formed in the full 0.2–10 keV energy band from events of ASCA grades 0, 2, 3, 4 and 6. Source detection was carried out with the CIAO task WAVDETECT, with wavelet scale sizes of 1, 2, 4 and 8 pixels and a false-positive probability threshold of 10^{-5} .

2.2 *XMM-Newton*

ULAS J1120+0641 was observed over three *XMM-Newton* orbits between 2012 May 23 and June 21 for a total observing time of 331 ks. The European Photon Imaging Cameras (EPICs) were operated in full-frame mode, with thin filters. EPIC data were processed using the *XMM-Newton* SCIENCE ANALYSIS SOFTWARE (SAS) version 12.0.1 (Gabriel et al., 2012). Times of high particle background were excluded by inspection of lightcurves in the 5–12

keV energy range, leading to total exposure times of 226, 223 and 174 ks in the MOS1, MOS2 and pn cameras respectively. Images were constructed in four bands: 0.2–0.5 keV, 0.5–2 keV, 2–5 keV and 5–10 keV. Background images were produced following the procedure described in Loaring et al. (2005). The images were then source-searched in the four energy bands simultaneously using the standard SAS tasks EBOXDETECT and EMLDETECT, again following the procedure described in Loaring et al. (2005).

We extracted a spectrum of ULAS J1120+0641 following the procedure described in Page et al. (2006), in this case extracting source counts from an 11 arcsec radius region around the target in each detector. This source-extraction region includes 60–70 per cent of the photons for a point source such as ULAS J1120+0641, the precise fraction depending on photon energy and EPIC camera. The small aperture is chosen to minimise the background contribution to the spectrum of this very faint source. The enclosed energy fraction is taken into account in the generation of the response files by the standard SAS task ARFGEN. Event patterns 0–12 were included in the MOS cameras, while for the pn camera we used patterns 0–4 above 0.4 keV and only pattern 0 between 0.2 and 0.4 keV. Channels containing strong instrumental emission lines were excluded. The spectra of the target from the different observations and different EPIC cameras were then combined to form a single spectrum, and the corresponding response matrices and background spectra were combined in an appropriate fashion to form a single response matrix and a single background spectrum, following the method described in Appendix A of Page, Davis & Salvi (2003). Finally, the spectrum was grouped to a minimum of 20 counts per bin.

3 RESULTS

In the WAVDETECT source search of the 0.2–10 keV *Chandra* ACIS image a point-like source is found within 0.5 arcsec of ULAS J1120+0641 at equatorial coordinates 11 20 01.50 +06 41 23.9 (see Fig. 1). The source has a 1σ position uncertainty of 0.4 arcsec and so its position is consistent with that of ULAS J1120+0641. The source is formed of 7 net counts (to 1 background count), according to the WAVDETECT algorithm, implying $7.0^{+4.0}_{-2.8}$ net source counts if we adopt the 68 per cent Poisson confidence limits described in Gehrels (1986). We have verified the source-count measurement by manual inspection of the ACIS image, finding 8 counts in the image within a 1 arcsec radius aperture around the source, and an average background level in the surrounding image that corresponds to 0.7 counts in an aperture of this size. No other X-ray sources are found within 30 arcsec of ULAS J1120+0641, so we do not expect issues with source blending in the larger point-spread function of *XMM-Newton*.

In the *XMM-Newton* EPIC images, an X-ray source is again found with a position consistent with ULAS J1120+0641: 1.7 arcsec distance, with a 1σ position uncertainty of 1.3 arcsec (see Fig. 1). The source is detected with 114 net source counts, in the full 0.2–10 keV energy range with a false source probability of 1.6×10^{-10} , equivalent to 6.4σ . It is detected individually in the 0.2–0.5 keV and 0.5–2.0 keV bands with fluxes of $6.2 \pm 1.7 \times 10^{-16} \text{ erg s}^{-1} \text{ cm}^{-2}$ and $5.7 \pm 1.2 \times 10^{-16} \text{ erg s}^{-1} \text{ cm}^{-2}$ respectively. It is not detected above 2 keV, and 3 sigma upper limits are obtained of $4.1 \times 10^{-16} \text{ erg s}^{-1} \text{ cm}^{-2}$ for the 2–5 keV flux and $4.2 \times 10^{-16} \text{ erg s}^{-1} \text{ cm}^{-2}$ for the 5–10 keV flux.

The X-ray spectrum of ULAS J1120+0641 obtained from the EPIC data is shown in Fig. 2. The spectrum was fitted with a power

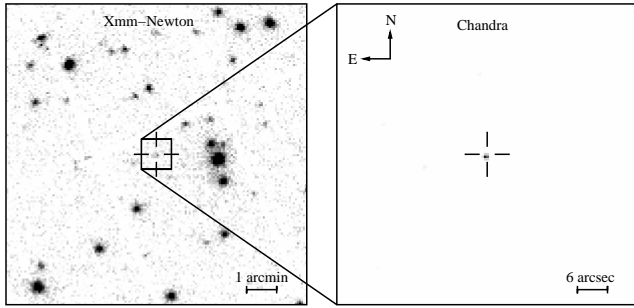


Figure 1. The left panel shows the *XMM-Newton* EPIC image centred on ULAS J1120+0641 in 0.2-2.0 keV, formed by summing the 0.2-0.5 keV and 0.5-2.0 keV images described in Section 2.2. The right panel shows the central arcminute of the *Chandra* image, after adaptive smoothing with the CIAO task DMIMGADAPT. In both panels the cross hairs mark the near-IR position of ULAS J1120+0641 from Mortlock et al. (2011)

law model, with fixed Galactic absorption. The best fit spectral index is $\alpha = 1.64^{+0.37}_{-0.33}$. The fit is acceptable, with a χ^2 of 20.4 for 15 degrees of freedom². The contribution of each channel to the χ^2 is shown in the bottom panel of Fig. 2. There are no deviations from the best-fit model which are individually significant, and there is no systematic shape to the χ^2 contributions which might justify a more complex model. The rest-frame 2-10 keV luminosity implied by the fit is $4.7 \pm 0.9 \times 10^{44}$ erg s⁻¹.

A common measure of the UV to X-ray spectral shape in AGN is the power law slope α_{OX} that would connect the flux densities at 2,500 Å and 2 keV in the rest frame of the source. For ULAS J1120+0641, restframe 2,500 Å falls at 20,213 Å, in the near-IR in the observed frame. We measure the flux density at this wavelength from the near-IR spectrum presented in Mortlock et al. (2011) to be $3.5 \pm 0.4 \times 10^{-18}$ erg s⁻¹ cm⁻² Å⁻¹. An energy of 2 keV in the restframe of ULAS J1120+0641 falls at 0.247 keV in the observed EPIC spectrum. We obtain the 0.247 keV flux and the uncertainty in this value directly from the power-law fit to the EPIC spectrum. Assuming that the rest-frame ultraviolet emission was the same at the time of the *XMM-Newton* observation as it was at the time of the near-IR observations, we find $\alpha_{OX} = 1.76 \pm 0.07$, where the uncertainty is dominated by the uncertainty on the 0.247 keV flux.

To compare the X-ray flux between the *Chandra* and *XMM-Newton* observations, we note that the X-ray flux and spectrum of ULAS J1120+0641 are characterised much better in the *XMM-Newton* observation than in the *Chandra* observation. An appropriate way to perform the comparison is therefore to use the parameters from the spectral fit to the *XMM-Newton* spectrum to estimate the number of counts that would be expected in the *Chandra* observation, for comparison to the observed number of counts. For this, we use version 4.6b of the PORTABLE, INTERACTIVE MULTI-MISSION SIMULATOR (PIMMS; Mukai, 1993). The best-fit parameters from the *XMM-Newton* spectrum, correspond to an expected 1.9 source counts from ULAS J1120+0641 in the 0.2-10 keV band *Chandra* S3 image, and the uncertainties in the *XMM-Newton* spectrum translate to an uncertainty of 20 per cent in the predicted number of *Chandra* counts.

Including the background level in the *Chandra* image (1 count

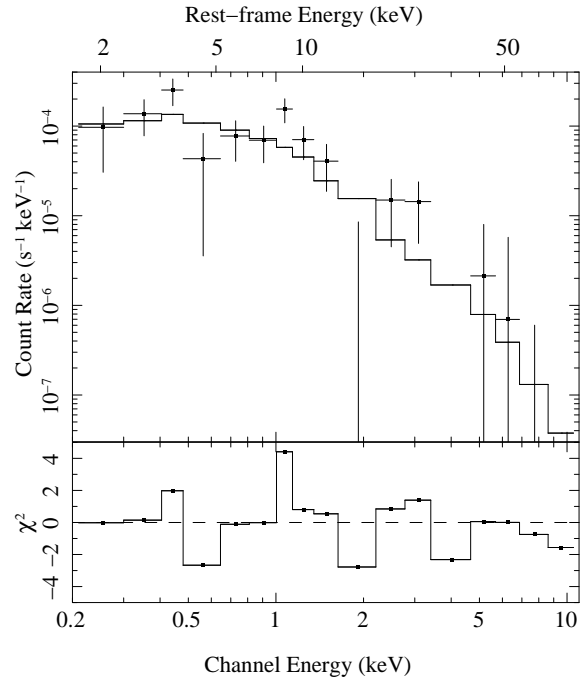


Figure 2. *XMM-Newton* EPIC spectrum of ULAS J1120+0641. The upper panel shows the observed counts spectrum (datapoints) together with the best fit power-law spectral model, with $\alpha = 1.64$ and Galactic $N_H = 5.07 \times 10^{20}$ cm⁻². The lower panel shows the contribution of each bin to the total χ^2 multiplied by the sign of (data – model).

in the WAVDETECT cell), we would predict a total of 2.9 ± 0.4 counts at the position of ULAS J1120+0641 in the *Chandra* image, compared to a total of 8 counts observed. Assuming Poisson statistics, the probability of observing 8 or more counts for an expectation of 2.9 counts is only 0.01, providing strong evidence that ULAS J1120+0641 has decreased in X-ray flux in the 15 months between the *Chandra* and *XMM-Newton* observations (< 2 months in the rest frame of the quasar). Comparable variability, while not the norm, has been observed before in high redshift quasars (e.g. Shemmer et al., 2005). Assuming the best-fit *XMM-Newton* spectrum, the count rate measured in the *Chandra* image corresponds to a rest-frame 2-10 keV luminosity of $1.8^{+1.0}_{-0.7} \times 10^{45}$ erg s⁻¹, and if we assume that the rest-frame ultraviolet flux is the same at the times of the near-IR and X-ray observations we obtain $\alpha_{OX} = 1.54^{+0.09}_{-0.08}$ at the time of the *Chandra* observation.

We also searched for variability during the month in which the *XMM-Newton* observations were carried out. We measured the count rate in the 0.2-2.0 keV range, in the three *XMM-Newton* observations separately. The three count rates are all within 1σ of the mean count rate; hence there is no evidence for variability during the *XMM-Newton* observation period.

Finally, we have examined the optical counterparts to the X-ray sources found with *XMM-Newton* and *Chandra* within a 200 arcsec radius of ULAS J1120+0641, where we have deep z -band and Y -band near-IR imaging, to see if any are likely to be at the same redshift as the quasar. None of the candidates brighter than $Y=20.5$ have sufficiently red $z - Y$ colours to indicate a redshift $z \sim 7$, and so there is no evidence for X-ray sources which are in a common large-scale structure with ULAS J1120+0641. The X-ray

² Given the relatively small number of counts, we have also performed the fitting using the C -statistic (Cash, 1979) instead of χ^2 , and obtain a very similar best-fit slope of $\alpha = 1.58^{+0.30}_{-0.35}$.

sources within 200 arcseconds of ULAS J1120+0641 are likely to be unrelated AGN at lower redshifts.

4 DISCUSSION

There is a well-documented linear correlation between α_{OX} and log UV luminosity, such that the most UV-luminous quasars have the largest values of α_{OX} , and hence the largest ratios of UV to X-ray luminosity (e.g. Strateva et al., 2005; Steffen et al., 2006; Just et al., 2007; Vasudevan et al., 2009; Wu, 2012). According to the relation given by Just et al. (2007), and translating the monochromatic 2,500 Å luminosity of ULAS J1120+0641 (3.5×10^{31} erg s⁻¹ Hz⁻¹) to the cosmology assumed by Just et al. (2007), we would predict a value of $\alpha_{OX} = 1.71 \pm 0.14$ for ULAS J1120+0641, where the uncertainty represents the observed dispersion around the relation. The value of $\alpha_{OX} = 1.76 \pm 0.07$ obtained from the *XMM-Newton* observation is thus consistent with the value expected, and α_{OX} is still consistent with the prediction if the X-ray flux is increased to the level suggested by the *Chandra* observation.

On the other hand, the X-ray spectral slope found for ULAS J1120+0641, $\alpha = 1.64_{-0.33}^{+0.37}$, is somewhat softer than the mean found for lower redshift quasars. For optically-selected quasar samples with mean redshifts below 2, observed with *XMM-Newton*, Young, Elvis & Risaliti (2009) and Scott et al. (2011) obtained mean values for α of $\langle \alpha \rangle = 0.90$ and $\langle \alpha \rangle = 0.99$ with intrinsic dispersions of $\sigma_\alpha = 0.40$ and $\sigma_\alpha = 0.30$ respectively. Similarly, studies of X-ray-selected quasar samples with mean redshifts below 2 generally find $0.89 < \langle \alpha \rangle < 1.00$, with dispersions around the mean ranging from $\sigma_\alpha = 0.2$ to $\sigma_\alpha = 0.36$ (e.g. Mateos et al., 2005; Page et al., 2006; Mateos et al., 2010; Lanzuisi et al., 2013).

Arguably, samples of optically selected quasars form the best comparison samples for ULAS J1120+0641, given its discovery via rest-frame UV emission. Furthermore, given its large redshift such that emission below 2 keV in the rest frame is shifted below the *XMM-Newton* bandpass in the observed frame, spectral indices measured above 2 keV in the rest frame are the most appropriate for comparison with that of ULAS J1120+0641. Conforming to these two criteria, for data above 2 keV in the rest frame Piconcelli et al. (2005) find $\langle \alpha \rangle = 0.89$ for radio-quiet PG quasars, while Page et al. (2004) find $\langle \alpha \rangle = 0.90$ for their small sample of luminous, optically-selected quasars. Similar to the comparison with X-ray selected samples, ULAS J1120+0641 has a softer X-ray spectrum than the average for optically selected quasars at lower redshift.

Moving now to high-redshift quasars, Grupe et al. (2006) examined the *XMM-Newton* observations of a sample of 21 quasars at $z > 4$. For the 10 radio-quiet objects in their sample which were detected with enough counts to permit spectral analysis, they obtained³ $\langle \alpha \rangle = 1.19 \pm 0.16$, and argued that this rather soft slope indicates that $z > 4$ quasars are accreting at a high fraction of the Eddington rate. On the other hand, Just et al. (2007) obtained $\langle \alpha \rangle = 0.93 \pm 0.16$ for a sample of $z > 4$ radio quiet quasars using a combination of *XMM-Newton* and *Chandra* data, and Shemmer et al. (2006) found $\langle \alpha \rangle = 0.95_{-0.26}^{+0.30}$ for their sample of 15 $z > 5$ radio-quiet quasars using *Chandra* observations. Both

of these samples yield X-ray spectral slopes which are indistinguishable from quasar samples at lower redshift. For the individual $z = 6.3$ radio-quiet quasar SDSS J1030+0524, Farrah et al. (2004) found $\alpha = 1.12 \pm 0.11$, and argued that neither this quasar, nor other high-redshift quasars which had been studied at that time, could be distinguished from quasars at lower redshifts by their X-ray spectra. ULAS J1120+0641 however has a softer X-ray spectrum than is typical for any of these samples.

It is well established (Pounds, Done & Osborne, 1995; Leighly, 1999) that X-ray spectral indices $\alpha > 1$ are associated with large ratios of L/L_{Edd} where L is bolometric luminosity and L_{Edd} is Eddington luminosity. Indeed, it has been proposed that α can be used as an estimator of L/L_{Edd} by using the linear correlation between $\log(L/L_{\text{Edd}})$ and α (Shemmer et al., 2008). Substituting the measured α for ULAS J1120+0641 into the expression relating α and L/L_{Edd} given by Equation 1 of Shemmer et al. (2008), or the equivalent expressions from later works (Risaliti et al., 2009; Jin et al., 2012; Brightman et al., 2013) suggests that ULAS J1120+0641 may be accreting at several times the Eddington rate. For example, adopting the expression from Jin et al. (2012), and deriving the overall uncertainty by adding the measurement error on α to the intrinsic dispersion of α about the relation in quadrature, we obtain $L/L_{\text{Edd}} = 5_{-4}^{+15}$.

Since our X-ray observations suggest that $L/L_{\text{Edd}} > 1$, and moderate levels of super-Eddington accretion are consistent with the range of L/L_{Edd} estimated from the UV luminosity / emission-line-derived black-hole mass of ULAS J1120+0641 ($L/L_{\text{Edd}} = 1.2_{-0.5}^{+0.6}$ Mortlock et al., 2011) we briefly explore how super-Eddington accretion might impact our understanding of this object.

First, we consider the unusually small ionized near-zone around ULAS J1120+0641. Bolton et al. (2011) show that the quasar cannot have been shining at its present UV brightness for significantly more than 10^7 years, which is only one fifth of a characteristic e-folding timescale of 5×10^7 years for Eddington-limited accretion. The e-folding timescale is inversely proportional to L/L_{Edd} , so the discrepancy between the two timescales is reduced by a factor of 2 if $L/L_{\text{Edd}} = 2$.

Second, we examine the implications of super-Eddington accretion for the constraints on the seed black hole. Considering that the bolometric luminosity of the quasar is rather better determined than its black hole mass, we can take the black hole mass to scale inversely with L/L_{Edd} ; adopting the luminosity and mass estimates from Mortlock et al. (2011), this implies $M_{\text{BH}} = 2.4(L_{\text{Edd}}/L) \times 10^9 M_\odot$. More importantly, the e-folding timescale is inversely proportional to L/L_{Edd} , implying a larger ratio of final to seed black hole mass for higher L/L_{Edd} . For reference, we would require seed black holes of $5.6 \times 10^3 M_\odot$ and $2.7 \times 10^4 M_\odot$ for formation redshifts of $z = 30$ and $z = 20$ respectively if the quasar has had $L/L_{\text{Edd}} = 1$ since the formation of its seed. The assumption that the quasar has accreted continuously, and without significant off-periods, i.e. a duty cycle close to 1, would be unrealistic for quasars with $z < 3$, but is reasonable for quasars with $z > 4$ (Shankar, Weinberg & Shen, 2013). To have grown the black hole in ULAS J1120+0641 from a $100 M_\odot$ seed would require an average value of $L/L_{\text{Edd}} = 1.29$ over the lifetime of the quasar if the seed formed at $z = 30$ or $L/L_{\text{Edd}} = 1.46$ if the seed formed at $z = 20$. Such values of L/L_{Edd} are compatible with the observational constraints, hence ULAS J1120+0641 could have grown from the remnant of a Population III star, as well as from the remnant of a quasi-star, or from a collapsed stellar clus-

³ The uncertainty given here is the error on the mean, whereas Grupe et al. (2006) give the standard deviation.

ter (Begelman, Volonteri & Rees, 2006; Volonteri, 2012), if it has maintained such a rate of growth throughout its existence.

ACKNOWLEDGMENTS

This work is based in part on observations obtained with *XMM-Newton*, an ESA science mission with instruments and contributions directly funded by ESA Member States and NASA. This work is based in part on observations made by the *Chandra* X-ray Observatory and has made use of software provided by the *Chandra* X-ray Center in the application package CIAO.

REFERENCES

- Ahn C.P., et al., 2012, *ApJS*, 203, 21
- Begelman M.C., Volonteri M., Rees M.J., 2006, *MNRAS*, 370, 289
- Brightman M., et al., 2013, *MNRAS*, 433, 2485
- Bolton J.S., Haehnelt M.G., Warren S.J., Hewett P.C., Mortlock D.J., Venemans B.P., McMahon R.G., Simpson C., 2011, *MNRAS*, 416, L70
- Bromm V., Yoshida N., Hernquist L., McKee C.F., 2009, *Nature*, 459, 49
- Cash W., 1979, *ApJ*, 228, 939
- De Rosa G., et al., 2013, *MNRAS* submitted; arXiv:1311.3260v2
- Fan X., et al., 2006, *AJ*, 132, 117
- Farrar D., Priddey R., Wilman R., Haehnelt M., McMahon R., 2004, *ApJ*, 611, L13
- Fruscione et al., 2006, *Proc. SPIE* 6270, 62701
- Gabriel C., et al., 2012, Technical Report XMM-SOC-USR-TN-0019 Issue 1.1, XMM-Newton Science Analysis System 12.0 scientific validation
- Gehrels N., 1986, *ApJ*, 303, 336
- Grupe D., Mathur S., Wilkes B., Osmer P., 2006, *ApJ*, 131, 55
- Jin C., Ward M., Done C., 2012, *MNRAS*, 425, 907
- Just D.W., Brandt W.N., Shemmer O., Steffen A.T., Schneider D.P., Chartas G., Garmire G.P., 2007, *ApJ*, 665, 1004
- Kalberla P.M.W., Burton W.B., Hartmann Dap, Arnal E.M., Bajaja E., Morras R., Pöppel W.G.L., 2005, *A&A*, 440, 775
- Lanzuisi G., et al., 2013, *MNRAS*, 431, 978
- Leighly K., 1999, *ApJS*, 125, 317
- Loaring N.S., et al., 2005, *MNRAS*, 362, 1371
- Mateos S., et al., 2005a, *A&A*, 433, 855
- Mateos S., et al., 2010, *A&A*, 510, A35
- Momjian E., Carilli C.L., Walter F., Venemans B., 2014, *ApJ*, 147, 6
- Mukai K., 1993, *Legacy*, 3, 21
- Mortlock D.J., et al., 2011, *Nature*, 474, 616
- Page M.J., Davis S.W. & Salvi N.J., 2003, *MNRAS*, 343, 1241
- Page K.L., Reeves J.N., O'Brien P.T., Turner M.J.L., Worrall D.M., 2004, *MNRAS*, 353, 133
- Page M.J., et al., 2006, *MNRAS*, 369, 156
- Piconcelli E., Jimenez-Bailon E., Guinazzi M., Schartel, N., Rodriguez-Pascual P.M., Santos-Lleo M., 2005, *A&A*, 432, 15
- Planck Collaboration, 2013, *A&A* in press (arXiv:1303.5076)
- Pounds K.A., Done C., Osborne J.P., 1995, *MNRAS*, 277, L5
- Risaliti G., Young, M., Elvis M., 2009, *ApJ*, 700, L6
- Salpeter E.E., 1964, *ApJ*, 140, 796
- Scott A.E., Stewart G.C., Mateos S., Alexander D.M., Hutton S., Ward M.J., 2011, *MNRAS*, 417, 992
- Shankar F., Weinberg D.H., Shen Y., 2010, *MNRAS*, 406, 1959
- Shemmer O., Brandt W.N., Vignali C., Schneider D.P., Fan X., Richards G.T., Strauss M.A., 2005, *ApJ*, 630, 729
- Shemmer O., et al., 2006, *ApJ*, 644, 86
- Shemmer O., Brandt W.N., Netzer H., Maiolino R., Kaspi S., 2008, *ApJ*, 682, 81
- Steffen A.T., Strateva I., Brandt W.N., Alexander D.M., KoekoemoerA.M., Lehmer B.D., Schneider D.P., Vignali C., 2006, *AJ*, 131, 2826
- Strateva I.V., Brandt W.N., Schneider D.P., Vanden Berk D.G., Vignali C., 2005, *AJ*, 130, 387
- Vasudevan R., Mushotzky R.F., Winter L.M., Fabian A.C., 2009, *MNRAS*, 399, 1553
- Venemans B.P., et al., 2012, *ApJ*, 751, L25
- Volonteri M., 2012, *Science*, 337, 544
- Wu J., et al., 2012, *ApJS*, 201, 10
- Young M., Elvis M., Risaliti G., 2009, *ApJS*, 183, 17